Molecular basis of differential receptor usage for naturally occurring CD55-binding and -nonbinding coxsackievirus B3 strains

Qingling Wang[a,b,c,1], Qian Yang[d,1], Congcong Liu[e,f,1], Guoqing Wang[g], Hao Song[h], Guijun Shang[i], Ruchao Peng[b], Xiao Qu[b], Sheng Liu[b], Yingzi Cui[b], Peiyi Wang[e], Wenbo Xu[d], Xin Zhao[b], Jianxun Qi[b], Mengsu Yang[a], and George F. Gao[a,b,2]

[a]Department of Biomedical Sciences, City University of Hong Kong, Hong Kong SAR, China; [b]CAS Key Laboratory of Pathogen Microbiology and Immunology, Institute of Microbiology, Chinese Academy of Sciences (CAS), Beijing 100101, China; [c]Shaanxi Natural Carbohydrate Resource Engineering Research Center, College of Food Science and Technology, Northwest University, Xi'an 710069, China; [d]World Health Organization Western Pacific Region (WHO WPRO) Regional Polio Reference Laboratory and National Health Commission Key Laboratory for Medical Virology, National Institute for Viral Disease Control and Prevention, Chinese Center for Disease Control and Prevention, Beijing 102206, China; [e]Cryo-EM Centre, Department of Biology, Southern University of Science and Technology, Shenzhen 518055, China; [f]Institute for Hepatology, National Clinical Research Center for Infectious Disease, Shenzhen Third People's Hospital, Shenzhen 518112, China; [g]Department of Pathogenobiology, The Key Laboratory of Zoonosis, Chinese Ministry of Education, College of Basic Medical Science, Jilin University, Changchun 130021, China; [h]Research Network of Immunity and Health, Beijing Institutes of Life Science, Chinese Academy of Sciences, Beijing 100101, China; and [i]Shanxi Academy of Advanced Research and Innovation, Taiyuan 030032, China

Contributed by George F. Gao; received October 12, 2021; accepted December 13, 2021; reviewed by Yao Cong and Pablo Guardado Calvo

Receptor usage defines cell tropism and contributes to cell entry and infection. Coxsackievirus B (CVB) engages coxsackievirus and adenovirus receptor (CAR), and selectively utilizes the decay-accelerating factor (DAF; CD55) to infect cells. However, the differential receptor usage mechanism for CVB remains elusive. This study identified VP3-234 residues (234Q/N/V/D/E) as critical population selection determinants during CVB3 virus evolution, contributing to diverse binding affinities to CD55. Cryoelectron microscopy (cryo-EM) structures of CD55-binding/nonbinding isolates and their complexes with CD55 or CAR were obtained under both neutral and acidic conditions, and the molecular mechanism of VP3-234 residues determining CD55 affinity/specificity for naturally occurring CVB3 strains was elucidated. Structural and biochemical studies in vitro revealed the dynamic entry process of CVB3 and the function of the uncoating receptor CAR with different pH preferences. This work provides detailed insight into the molecular mechanism of CVB infection and contributes to an in-depth understanding of enterovirus attachment receptor usage.

enteroviruses | differential receptor usage | cryo-EM | attachment or uncoating | entry

Enteroviruses (EV-Bs) consisting of coxsackievirus B1 to B6, coxsackievirus A9, echoviruses, and other newly identified enteroviruses are the main causative agents of aseptic meningitis and several acute diseases (1). Among these, globally distributed coxsackievirus B3 (CVB3) is a significant human pathogen causing myocarditis, aseptic meningitis, acute flaccid paralysis, hand–foot–mouth disease (HFMD), and pancreatitis and is also associated with type I diabetes through persistent infection and inflammation of pancreatic β-cells (2–6). In the United States, ∼10 to 15 million CVB3 infections per year were reported between 2014 and 2016 (7). A study in Yantai, China, found that CVB3 infections were widespread, with a seroprevalence rate of 52.3% (6). Additionally, repeated aseptic meningitis and myocarditis outbreaks, including fatal cases caused by CVB3, have increasingly been reported in Spain (8).

Receptor usage can define cell tropism and may be related to viral pathogenicity. Thus, understanding the receptor usage mechanism for CVB3 will provide a basis for rational drug and vaccine design against these viral infections. Enteroviruses enter cells by a dual-receptor system. In this system, an attachment receptor enables the virus to bind to the cell surface. Subsequently, the uncoating receptor induces conformational changes and facilitates the release of the genome from the viral particles into the cytosol of the host cell (9–11). In some cases, both steps can be accomplished by a single bifunctional receptor (12, 13). For EV-B, the neonatal Fc receptor and the coxsackievirus and adenovirus receptor (CAR), as uncoating receptors for Echo and CVB-related serotypes, respectively, are essential for viral entry (11, 14–16). CD55, as the attachment receptor, is utilized selectively for some CVB stereotypes, including CVB1, B3, and B5; some Echo serotypes, including echovirus 3, 6, 7, 11 to 13, 19 to 21, 25, 29, and 30; and several other enterovirus serotypes that include coxsackievirus A21 and enterovirus 70 (11, 17). As RNA viruses, enteroviruses naturally have high mutational rates, resulting in viral genome diversity at the population level, which affects their receptor-binding properties (18–20). Previous biochemical studies indicated that several CD55-nonbinding EV-Bs could

Significance

Receptor usage can affect cell tropism and viral pathogenicity. CVB causes viral-induced heart disease, aseptic meningitis, and many other severe diseases globally that can engage CAR in host cells and selectively utilizes CD55 to infect them. However, the mechanism of CVB differential receptor usage and its dynamic entry into cells remains poorly understood. This study elucidates the molecular mechanism of VP3-234 residues as critical population selection determinants influencing CD55 affinity/specificity for naturally occurring CVB3 strains. Moreover, the demonstration that CAR facilitates viral uncoating with strain-dependent pH preferences suggests that the entry and infection of different enterovirus strains vary with the extent of pH dependence. Altogether, these findings expand our understanding of nonenveloped virus infections and provide clues for therapeutic interventions.

Author contributions: G.F.G. designed research; Q.W., Q.Y., C.L., X.Q., and S.L. performed research; G.W., P.W., and W.X. contributed new reagents/analytic tools; Q.W., C.L., H.S., G.S., R.P., and J.Q. analyzed data; and Q.W., Q.Y., C.L., Y.C., X.Z., J.Q., M.Y., and G.F.G. wrote the paper.

Reviewers: Y.C., Chinese Academy of Sciences; and P.G.C., Institut Pasteur.

The authors declare no competing interest.

This article is distributed under Creative Commons Attribution-NonCommercial-NoDerivatives License 4.0 (CC BY-NC-ND).

[1]Q.W., Q.Y., and C.L. contributed equally to this work.

[2]To whom correspondence may be addressed. Email: gaof@im.ac.cn.

This article contains supporting information online at http://www.pnas.org/lookup/suppl/doi:10.1073/pnas.2118590119/-/DCSupplemental.

Published January 19, 2022.

obtain CD55-binding ability after passages in rhabdomyosarcoma cells (21, 22).

Differential receptor usage represents a selective evolutionary mechanism favoring virus survival. However, knowledge of receptor usage for epidemic isolate distribution in distinct areas is limited. Enteroviruses commonly initiate infection in the intestinal epithelium, where attachment receptor usage can enhance infection efficiency (23). There has not been a systematic analysis of attachment receptor usage of EV-Bs. Herein, CVB3, a serotype with both CD55-binding and -nonbinding strains, was used as the model system to decipher the underlying evolutionary mechanism of attachment receptor usage and its dependency on the proportion and geographic distribution of clinical isolates.

The uncoating receptor is responsible for viral capsid dissociation and genome release, which are essential to complete the viral life cycle after virus attachment to the host cell (9). The natural lipid "pocket factor," which is harbored in the hydrophobic pocket of the viral protein 1 (VP1) subunit, is a hypothetical trigger to initiate the uncoating process (9, 10). Receptor binding and/or low pH in the endosomal system can induce viral uncoating (17). For most enteroviruses, including EV71 (24), CVA10 (12), and Echo 6 (11), both receptor binding and exposure to low pH in the endosomal system could cause pocket factor extrusion, followed by the formation of an expanded uncoating intermediate (A particle) by the opening of a channel near the icosahedral twofold axis and subsequent genome release. Recent findings indicate that receptor binding under neutral pH for some enteroviruses can also trigger viral uncoating (16, 25, 26). As the cell-adhesion molecule found in tight junctions, CAR has been previously identified as a universal uncoating receptor for CVB and plays a crucial role in CVB-related pathology (27). A previous study indicated that CAR could induce CVB3 conformational changes, forming a CAR-mediated uncoating intermediate termed the "A particle" at pH 6.0 (15). A systematic study of high-resolution uncoating molecular events of distinct CVB3 isolates under both pH conditions could provide in-depth insights into the mechanisms of enterovirus infection.

In this study, a series of atomic-resolution cryoelectron microscopy (cryo-EM) structures of CD55-binding and -nonbinding CVB3 isolates were determined in the apo form and in complex form with their receptor CD55 or CAR under both neutral and acidic pH conditions. The findings indicate that CAR facilitates the CVB3 uncoating process with strain-dependent pH preferences. Notably, the molecular mechanism of single–amino acid differences in naturally occurring CVB3 clinical strains determining the binding affinity/specificity to CD55 was elucidated. Additionally, a necessary criterion to assess receptor usage of CVB3 isolates for surveillance and clinical control was provided.

Results

Clinical CVB3 Isolates Are Diversified at the VP3-234 Site. To dissect the molecular mechanism of differential receptor usage among natural enterovirus strains, CVB3 was used as a model system for a comprehensive analysis. From 2012 to 2017, 20 clinical CVB3 isolates of infants and children under 6 y of age with HFMD were collected from different provinces in China. The isolates were identified and the *VP1* nucleotide sequences from these CVB3 strains were deposited in the National Center for Biotechnology Information (NCBI) database (*SI Appendix*, Table S1). These sequences, along with another 95 CVB3 sequences from the GenBank database, were investigated and analyzed. A phylogenetic tree was constructed. These isolates were assigned to five groups (A to E), with at least 15% nucleotide divergence between the different groups (*SI Appendix*, Fig. S1*A*). Groups A and E comprised CVB3 sequences from the United States, Germany, Australia, and France. Group D mainly comprised samples from China, and Group C mainly from India.

To explore the mechanism of differential receptor usage, amino acid distribution probability was analyzed at each site for VP1, VP2, and VP3 sequences available in the NCBI database and from our isolates (Fig. 1 *A*–*C*). Most amino acids in all three VP proteins were conserved (Fig. 1 *A*–*C*). Compared with VP1 or VP2 proteins, VP3 residues were more conserved, except for VP3-35, VP3-58, VP3-78, VP3-234, and VP3-235 sites (Fig. 1*C*). Five different amino acids were present in the VP3-234 site for all 89 available VP3 sequences. They were dominated by Q (41.6%), followed by D (37.1%), V (12.3%), and E (7.9%). Only one strain possessed VP3-234N. CVB3 epidemic strains varied among different areas and populations. VP3-234D was only detected in Asia, whereas VP3-234Q was predominantly collected from Europe, the United States, and Australia (Fig. 1 *D* and *E*). VP3-234Q was mainly distributed in phylogenic groups A, C, and E. VP3-234D was only distributed in group D (*SI Appendix*, Fig. S1 *B*–*F*).

Direct Binding of Receptors to CVB3 Isolates. As previously reported, a single–amino acid change in VP3-234, VP1-271, or VP2-138 sites could affect CVB3 interaction with CD55 (21, 28). VP3-234 sites exhibited amino acid diversity for naturally occurring CVB3 isolates (Fig. 1*C*). Hence, it is reasonable to speculate that VP3-234 sites more likely serve as population selection determinants contributing to CD55 availability during CVB3 evolutionary adaptation. Therefore, CVB3/MKP3 (VP3-234Q), CVB3/XJ12-36/XJ/CHN/2012 (VP3-234N), CVB3/GS12-55/GS/CHN/2012 (VP3-234V), CVB3/HuN16-54/HuN/CHN/2016 (VP3-234D), and CVB3/XZ17-10/XZ/CHN/2017 (VP3-234E) were chosen for further analysis. They were designated as CVB3Q, CVB3N, CVB3V, CVB3D, and CVB3E, respectively. Full isolate particles were purified by sucrose density centrifugation. For the two receptors, the soluble extracellular D1 and D2 domains of the human CAR protein and the extracellular domain of the human CD55 protein were expressed and purified (11, 15). Surface plasmon resonance (SPR) experiments were performed to investigate the interactions between varied CVB3 strains and CD55 or CAR.

No binding affinity was detected between CVB3E and CD55 (Fig. 2*A*). In contrast, the other four CVB3 isolates (CVB3Q, CVB3N, CVB3V, and CVB3D) could interact with CD55 with dramatic differences in their binding affinities. The highest binding affinity was observed for CVB3Q (K_D 465 nM), and ~17- and 22-fold lower binding affinities were observed for CVB3N (K_D 7.8 μM) and CVB3V (K_D 10 μM), respectively (Fig. 2 *C*–*E*). A weaker binding affinity was detected for CVB3D (K_D 46 μM) (Fig. 2*B*). Empty CVB3Q particles were also tested. They exhibited no interaction with CD55 (Fig. 2*F*).

Unlike CD55, CAR could bind to all five CVB3 isolates (Fig. 2 *G*–*K*). The binding affinity between CAR and CVB3 was similar among the different isolates, and were all within one magnitude range (Fig. 2 *G*–*K*). CAR and CVB3 interactions exhibited micromolar binding affinity. The highest binding affinity was observed for CVB3Q (K_D 3.16 μM), and the lowest affinity was observed for CVB3N (K_D 34 μM). No discernible binding for CVB3Q empty virions was observed (Fig. 2 *G*–*L*).

Structural Mechanism of VP3-234 Residues Determining CD55 Binding Affinity/Specificity for Natural CVB3 Isolates. To further elucidate the differential receptor usage mechanism for naturally occurring CVB3 isolates, cryo-EM analysis was performed to determine the structures of CD55-binding CVB3Q, CVB3N, and CD55-nonbinding CVB3E, alone and in complex form with CD55 under neutral pH at the atomic level (2.5 to 3.7 Å) (Fig. 3 *A* and *B* and *SI Appendix*, Figs. S2 and S3 and Table S2). In general, the architecture of CVB3E viral particles highly

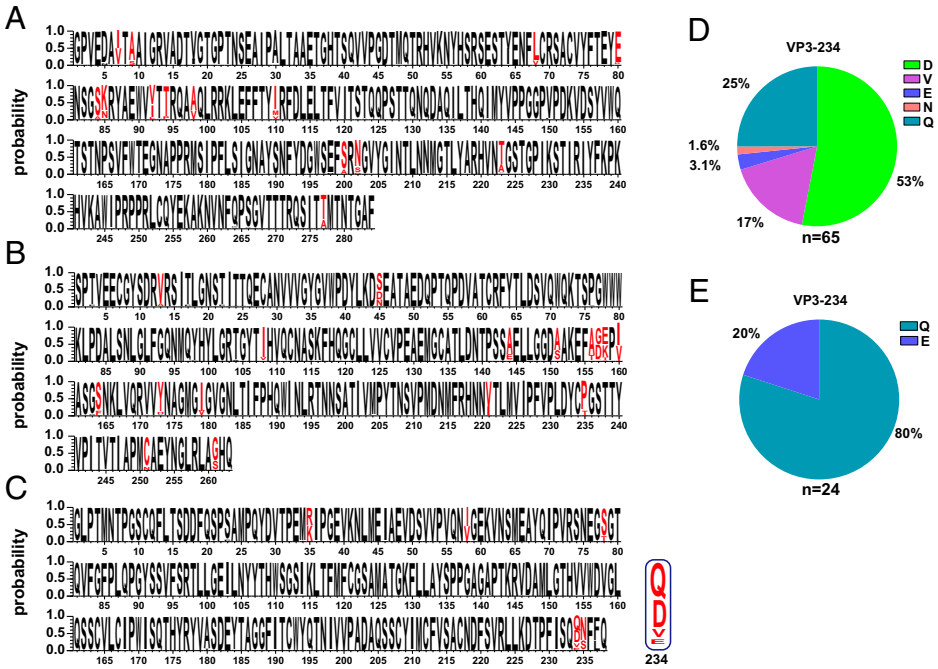

Fig. 1. Amino acid probability distribution of CVB3 surface proteins. (*A*–*C*) CVB3 sequences (n = 115) were collected and aligned. Of the 115 sequences, 95 were available in the NCBI database and 20 were isolates collected from China from 2012 to 2017. Amino acid probability distribution on each site of VP1 (*A*), VP2 (*B*), and VP3 (*C*) proteins. Variable residue sites are colored in red. (*D* and *E*) Percentage of CVB3 isolates according to the VP3-234 amino acid (Q/N//V/D/E) distribution (*D*) among 65 strains in Asia and other parts of the world (mainly Europe, the United States, and Australia) among 24 strains (*E*).

resembled that of the CVB3Q or CVB3N virions, with no obvious conformational changes among CVB3 virions, especially for the CD55-binding motifs (*SI Appendix*, Fig. S4). The overall structures of the CVB3–CD55 complexes showed that CD55 bridged across two adjacent protomers, involving VP1 and VP3 subunits within one protomer and the VP2 in both protomers (Fig. 3*C* and *SI Appendix*, Fig. S4*B* and Tables S3 and S4).

Based on a detailed analysis of the CVB3–CD55 interaction, it was observed that most interaction residues were located at nearly equivalent positions in CVB3Q and CVB3N capsid proteins (*SI Appendix*, Fig. S4*B*). More interactions between CD55 and CVB3Q were observed than those between CD55 and CVB3N (*SI Appendix*, Tables S3 and S4). Three major CD55-binding interfaces were observed in the VP1, VP2, and VP3 subunits in one protomer (Fig. 3*C*). For interface I and interface II, residues 264Q-271T and 254Q-257K of the CVB3-VP1 C-terminal loop and residue G59-N63 of CVB3-VP3 formed three binding patches with CD55-SCR2, thereby contributing to most of the strongly charged interactions (Fig. 3*D*). Among these residues, six equal hydrogen bonds were generated for CVB3Q–CD55 and CVB3N–CD55. Notably, residues 137L and 138D of CVB3-VP2 were responsible for minor interactions with CD55-SCR2 (*SI Appendix*, Tables S3 and S4), while residue 138D in CVB3N-VP2 hydrogen-bonded to the amidogen of Q115 of CD55-SCR2 (Fig. 3*D*). These features are consistent with previous biochemical evidence that VP1-271T and VP2-138D for CVB3 strains were required for virus attachment to CD55 (21, 28).

On the opposite side of CD55-SCR2 (interface III), the C terminus of VP3 further stabilized the interaction by contacting CD55-SCR2, which was critical for determining CD55 interaction for naturally occurring CVB3 virions (Fig. 3*C* and *SI Appendix*, Fig. S4*B*). Amino acid Q in VP3-234 site for CVB3 virion formed two hydrogen bonds, amino acid N in VP3-234 site formed one hydrogen bond, with the A122 backbone in CD55 (Fig. 3*D*). These interactions effectively anchored CD55 to the viral surface. More hydrogen-bonding interactions contributed to the higher affinity between CD55 and CVB3Q than that with CVB3N (Fig. 2 *D* and *E*).

Sequence alignment revealed that the VP3-234 sites in the binding interface showed the highest diversity among the selected strains and all available clinical NCBI strains (Fig. 1 *A*–*C* and *SI Appendix*, Fig. S4*B*). Detailed structural information revealed that VP3-234Q formed two hydrogen bonds with the A122 amidogen and carbonyl groups, while VP3-234N formed one hydrogen bond with the A122 amidogen group (Fig. 3*E*). Based on the cryo-EM structures, the single–amino acid substitution was modeled at the VP3-234 site. Negatively charged E234 or D234 could generate repulsive forces with the A122 carbonyl group, leading to an abolished or drastic decrease in CD55-binding capacity to CVB3 virions. Residue V234 possessed a small aliphatic side chain and could not form hydrogen bonds and did not display repulsive interactions, such as those of E234 or D234 residues with the A122 main chain (Fig. 3*E*). The findings of the structural analysis were consistent with the SPR results (Fig. 2 *A*–*E*).

CD55 is a universal receptor for several enteroviruses, and hence the binding sites and mechanisms of different CD55-binding enteroviruses were compared. The CD55-binding model with CVB3 was similar to that of Echo 6 but different from those of Echo 7, Echo 11, and Echo 12 (*SI Appendix*, Fig. S5*A*). Although a similar binding model between CD55 and Echo 6 or CVB3 was observed, the binding sites were different (*SI Appendix*, Fig. S5 *B* and *C*). The VP1 subunit of CVB3 interacted with the SCR2 domain of CD55; however, Echo 6 mainly used its VP2 subunit to bind to the SCR3 and SCR4 domains of CD55 (*SI Appendix*, Fig. S5 *B* and *C*). These results indicate that CD55-binding enteroviruses bind to different domains of CD55 using various binding sites on their capsids.

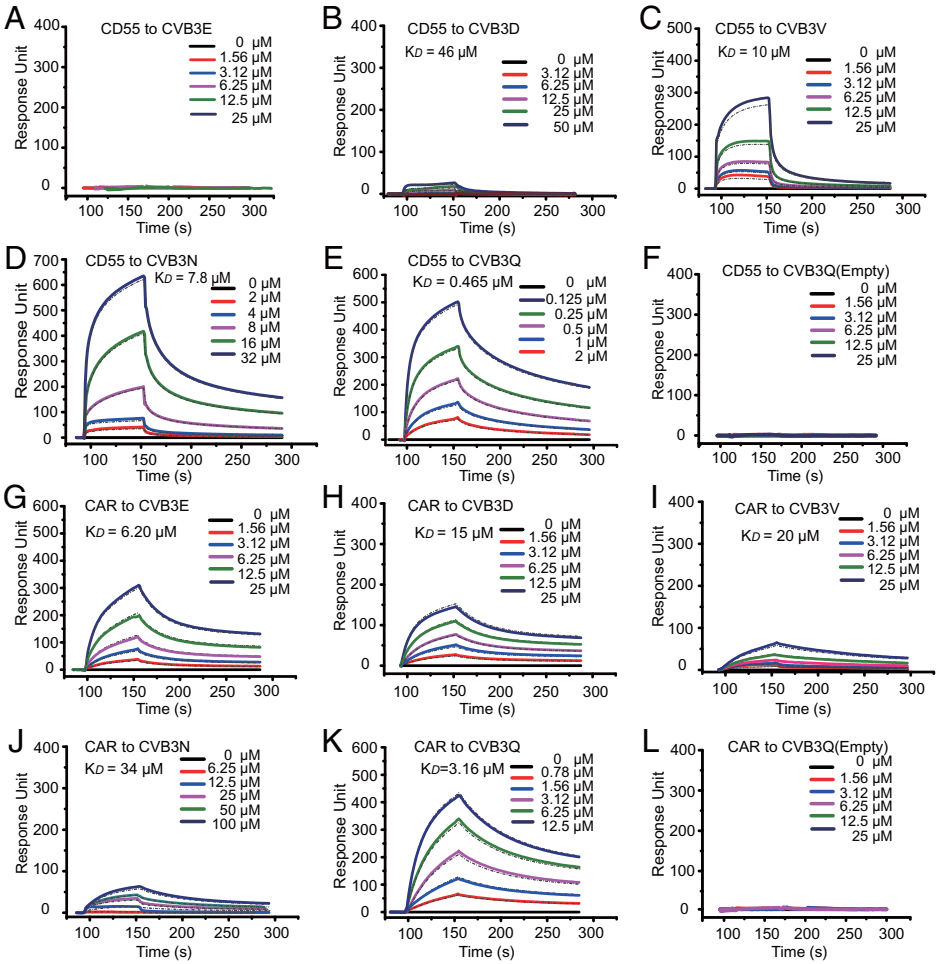

Fig. 2. Direct binding of CD55 or CAR to CVB3 isolates. (*A–F*) BIAcore diagrams of the soluble extracellular domain of CD55 bound to CVB3E (*A*), CVB3D (*B*), CVB3V (*C*), CVB3N (*D*), and CVB3Q (*E*) full particles at pH 7.4, with empty particles of CVB3Q as control (*F*). (*G–L*) BIAcore diagram of the soluble extracellular D1D2 domain of CAR bound to CVB3E (*G*), CVB3D (*H*), CVB3V (*I*), CVB3N (*J*), and CVB3Q (*K*) full particles at pH 7.4, with empty particles of CVB3Q (*L*) as control. K_D values were calculated using BIAcore 3000 analysis software (BIAevaluation version 4.1) and the fitting curves were labeled with a gray dotted line.

Structures of CVB3 Viruses with CAR. To further elucidate the diverse entry mechanisms of EV-B isolates, the complex structures of CVB3Q or CVB3E virions bound to CAR under both neutral and acidic conditions during different cell-entry stages at the atomic level (2.2 to 3.3 Å) were determined (Fig. 4 *A–F* and *SI Appendix*, Figs. S6 and S7 and Table S2).

Similar to other picornaviruses, within the CVB3 full virions or CD55-bound CVB3 virions, the pocket factor lipid molecule was well-accommodated in the pocket beneath the canyon of the VP1 subunit (*SI Appendix*, Fig. S8), which is critical for virion stability (9). Unlike the CVB3 full particles or CD55-bound CVB3 virions, the pocket factor was released in the CAR-bound CVB3Q and CVB3E virions (Fig. 4 *A–F* and *SI Appendix*, Fig. S8 *H*, *J*, and *K*). When incubated with CAR at pH 7.4 for 10 min on ice, the pocket factor was well-preserved in the CAR-bound CVB3Q capsid, with no obvious conformational change in the pocket (Fig. 4*G*). However, for the same incubation time, CVB3E already started its uncoating process, with the pocket factor being released from the capsid along with a slight downshift of the VP1 GH loop (residues 208 to 216) (Fig. 4 *I* and *J*), which is regarded as the gating loop responsible for receptor binding and pocket factor ejection in many enterovirus virions (11, 26). These results indicate that the binding of CAR, but not CD55, to CVB3 full virions can initiate viral uncoating, with slightly different efficiencies among CVB3 strains.

With an additional 10 min of incubation, the pocket factor was missing in CAR-bound CVB3Q viral particles at both pH 7.4 and 5.5, with an obvious downshift (~3.5 Å) of the VP1 GH loop, leading to collapse of the pocket (Fig. 4 *A–D* and *G*). For CAR-bound CVB3E virions that had lost the pocket factor, an additional 10-min interaction caused a deeper collapse of the pocket and a significant downshift (~3.0 Å) in the VP1 GH loop (Fig. 4 *I* and *J*). These observations are consistent with a probable universal mechanism for enterovirus uncoating, although the triggering factor for uncoating varies among different viruses (13, 16, 25).

CAR Facilitates the Uncoating Process of CVB3 Isolates with Diverse Efficiencies. Structural information indicated that CAR binding at pH 7.4 triggered the release of the pocket factor in both CVB3Q and CVB3E virions (Fig. 4 *A–F*). The uncoating process of CVB3Q and CVB3E was detected using the receptor-decorated liposome model under both neutral and acidic pH to explore whether the pH conditions affect capsid dissociation and subsequent genome release (*SI Appendix*, Fig. S9). CVB3Q particles were attached to CAR- and CD55-decorated liposome surfaces (*SI Appendix*, Fig. S9 *A* and *B*). CVB3E particles were attached only to the CAR-decorated surface but not to CD55-decorated liposomes (*SI Appendix*, Fig. S9 *C* and *D*), which was consistent with the SPR results (Fig. 2). After 60 min of

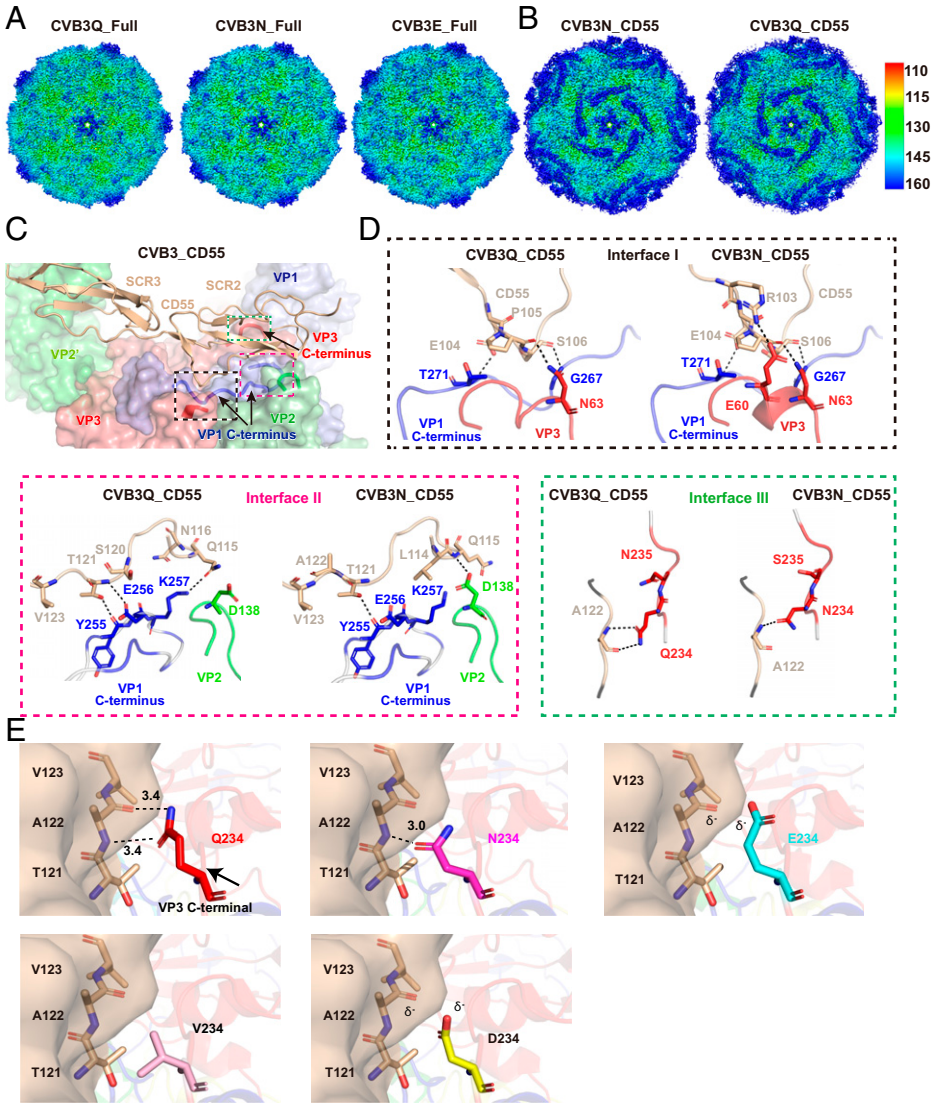

Fig. 3. Cryo-EM structures and detailed interactions among CVB3 viral particles and the CD55 receptor. (*A* and *B*) Density maps of CVB3Q (3.0 Å), CVB3N (2.7 Å), and CVB3E (2.5 Å) full particles (*A*), and complexes CVB3Q–CD55 (3.2 Å) and CVB3N–CD55 (3.0 Å) (*B*) at pH 7.4. The density map is colored by radius, as indicated in the legend bar. (*C*) Atomic model of the CVB3_CD55 three main contact interfaces, I, II, and III, indicated by a dashed rectangle in black, magenta, and green, respectively. The receptor is shown in ribbon models, and the viral protein is represented in surface models. (*D*) Interaction details between CVB3Q or CVB3N and CD55. (*E*) Hydrogen-bond interactions between A122 of CD55 with CVB3Q or CVB3N. Presumptive interaction of A122 of CD55 with VP3-234E, VP3-234V, and VP3-234D. VP3-234E or VP3-234D residues have the same electric charge as the A122 carbonyl group of CD55, marked δ^-. Interaction residues are shown in stick representation and hydrogen bonds are indicated by black dashed lines.

incubation at 37 °C, CVB3Q or CVB3E particles incubated with CD55-decorated liposomes or CD55 protein alone did not show a noticeable increase in empty particles (*SI Appendix*, Fig. S9 *A* and *C*). For both CVB3Q and CVB3E, a considerable proportion of empty particles was observed after incubation with CAR-decorated liposomes. Large numbers of empty particles were clearly arrested after CVB3Q particle incubation with CAR-decorated liposomes for 10 min (*SI Appendix*, Fig. S9*B*). Almost all CVB3Q full particles turned into empty particles and dropped down from liposomes under both pH conditions after 30 min of incubation (*SI Appendix*, Fig. S9*B*). The pH did not affect the uncoating efficiency of CVB3Q (*SI Appendix*, Fig. S9*E*). Compared with CVB3Q, 10 min of incubation with CAR-decorated liposomes did not lead to any apparent increase in the number of CVB3E empty particles (*SI Appendix*, Fig. S9*D*). A certain proportion of empty CVB3E particles was observed after 30 and 60 min of incubation under both pH conditions (*SI Appendix*, Fig. S9*D*). However, the percentage of CVB3E empty particles was significantly higher under acidic conditions (*SI Appendix*, Fig. S9*F*). These results indicate that CAR induced CVB3 uncoating with different efficiencies and strain-dependent pH preferences.

Discussion

Naturally Occurring Single–Amino Acid Variations May Affect Viral Pathogenicity. RNA viruses have high replication error rates. The resulting quasispecies may aid virus population survival in the presence of selective pressure, which also contributes to receptor-binding diversity (18, 20). The present study provides evidence demonstrating that highly variable VP3-234 residues are the molecular switches controlling CD55 binding for naturally occurring CVB3 strains during viral evolution. Additionally, three-dimensional structure analysis revealed that VP3-234 located on the VP3 protein C-terminal loop might be beneficial for altering CD55-binding characteristics (Fig. 3*E*). VP1 and

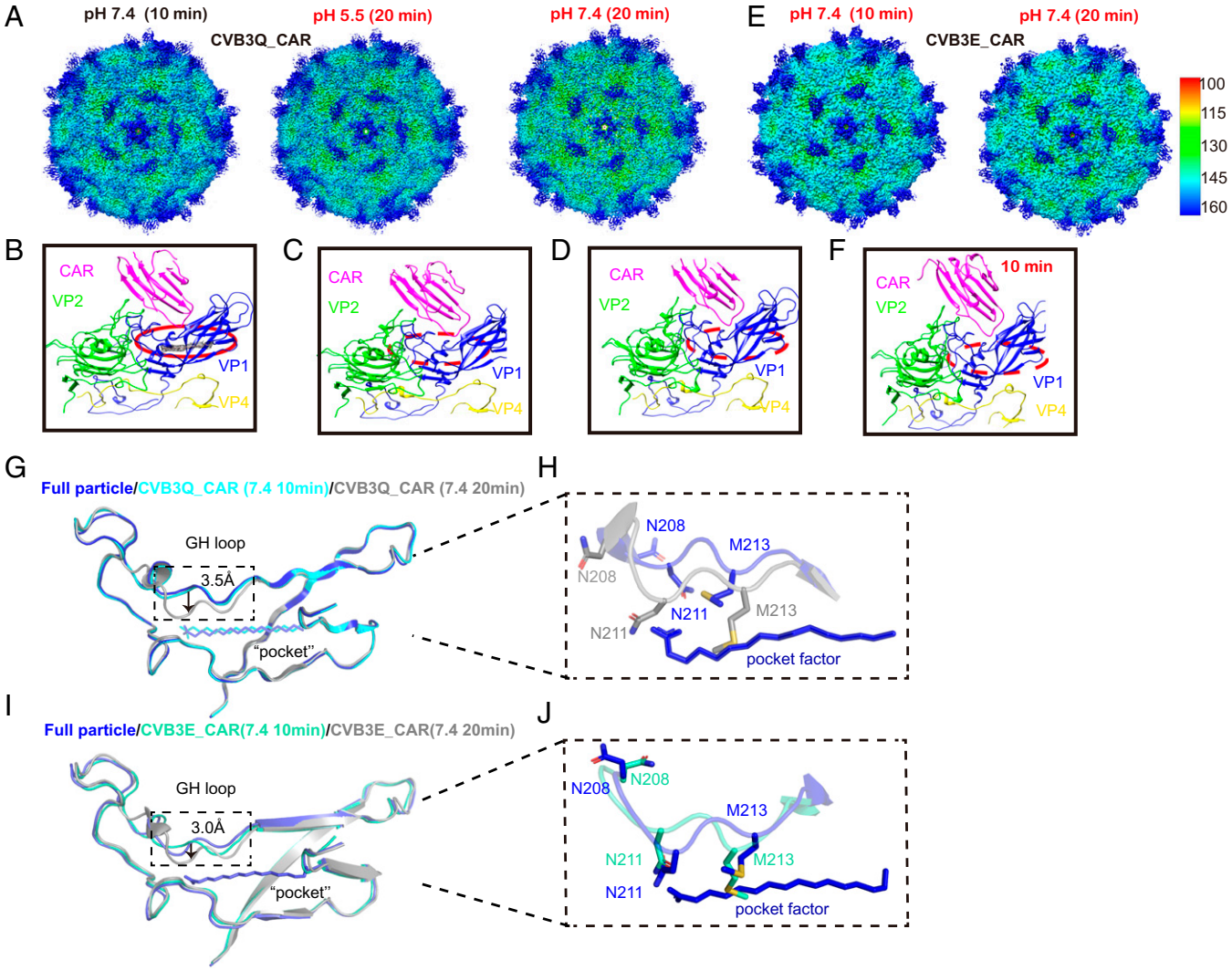

Fig. 4. Cryo-EM structures of the complex CVB3–CAR and structural changes surrounding the pocket. (*A–D*) Cryo-EM maps of the CVB3Q–CAR complex incubated for 10 min at pH 7.4 (3.2 Å), and an additional 10 min at pH 7.4 (3.2 Å) or 5.5 (2.8 Å) (*A*). The density map is colored by radius, as indicated by the legend bar. Close-up view of the pocket factor inside the CAR-bound CVB3Q particle for 10 min (*B*) and the corresponding pocket site in the group, with an additional 10-min incubation at both pHs (*C* and *D*). (*E* and *F*) Cryo-EM maps (*E*) of CVB3E–CAR complex incubation for 10 min (3.7 Å) and an additional 10-min incubation at pH 7.4 (2.2 Å). Close-up view of the pocket factor when the pocket is missing (*F*). (*G* and *I*) Conformational changes in the pocket region of CAR bound to CVB3Q (*G*) or CVB3E (*I*) particles upon 10- and 20-min incubations at pH 7.4. (*H* and *J*) Enlarged views of the major residues including N211, N212, and M213, highlighting the conformational change in the pocket region of the CVB3Q (*H*) and CVB3E (*J*) capsids.

VP2 proteins had several high–amino acid variability sites. These included VP1-85, VP1-92, VP1-110, VP1-200, VP1-202, VP1-223, VP1-277, VP2-45, VP2-144, VP2-151, VP2-157, VP2-158, and VP2-160. However, these residues did not participate in the CD55- and CVB3-binding interactions (Fig. 1 *A* and *B* and *SI Appendix*, Tables S3 and S4). Taken together, the findings provide an important criterion to assess whether a newly isolated clinical CVB3 strain can utilize CD55 to enter and infect cells.

CD55 as the complement inhibitory protein is broadly distributed and has recently attracted substantial attention due to its role in various diseases (29–32). Thus, whether a strain can utilize CD55 as the receptor for cell entry and infection is a factor that will affect the host tropism and immune response. Therefore, single–amino acid variations of VP3-234 sites for naturally occurring CVB3 isolates could possibly lead to differences in host immune response and viral virulence. Attachment receptors expressed on the host cell surface are believed to enhance viral infection by increasing the chance of encountering true receptors (11, 23). However, a previous study provided an unexpected answer to this question, suggesting that EV71 VP1-145G virus, which binds to heparan sulfate (HS), is less virulent than VP1-145E viruses, which cannot bind to HS. Hence, HS can act as a decoy to specifically trap VP1-145G viruses, leading to attenuated infection (33–35). However, this variation in human pathogenesis still requires more clinical samples to identify the relationship between CD55 affinity and symptoms of diseases caused by CVB3 infection. The present findings may also contribute to the selection of treatment programs based on patient needs.

Evolution and Geographic Distribution of CVB3 Variation in CD55 Binding. Amino acid diversity of VP3-234 sites (Q/N/V/D/E) is crucial for CD55 interaction affinity/specificity for different CVB3 isolates. The structural information and SPR results observed in the present study indicated that the neutral amino acids Q/N/V were capable of binding to CD55, whereas acidic residues D or E in VP3-234 sites generated charge repulsion with the A122 carbonyl group of CD55, leading to weak or undetectable CD55

binding affinity to the CVB3 virus (Figs. 2 *A–F* and 3*E*). Although the number of lysine residues was recognized as a major factor influencing the SPR results when using *N*-hydroxysuccinimide (NHS)–biotin as the biotinylation reagent, sequence analysis of VP1/VP2/VP3 proteins for CVB3Q/N/V/D/E virions indicated that it was unlikely that the number of lysine residues could determine the binding affinity between the CVB3 virion and its receptor (*SI Appendix*, Fig. S10).

More than 54% of CVB3 sequences from the NCBI database, and the recent isolates, had Q/N/V residues at VP3-234 sites. Among these, ∼46% harbored D or E residues (*SI Appendix*, Figs. S1 *B–F* and S11). Evolutionary pressure promoting the CD55-binding phenotype led to the tropism of some enteroviruses for new cell types (23). When specific sequences encoding VP3-234 were examined, single-nucleotide changes in E codons (GAA, GAG) resulted in D (GAU, GAC) and Q (CAA, CAG) codons (*SI Appendix*, Fig. S11). Thus, a single-nucleotide substitution was sufficient for E replacement with Q or D. However, mutations for E→V, E→N or Q→V, and Q→N required double-nucleotide substitutions. Therefore, N or V was more likely to be transformed directly from D, rather than from E, with D→V or D→N transformation enabling viruses to gain a higher CD55-binding capacity, according to the SPR analysis (Fig. 2 *A–F*). Notably, the CVB3 isolate in group D, mostly found in Asia, had more VP3-234 variations than those of any other groups. One possible reason was that more samples were analyzed from China. Alternatively, gene expression diversity for CVB3 receptors in different populations is possible.

Potential Mechanism of CVB3 Entry. Most enteroviruses and other picornaviruses utilize two types of receptors at different viral entry stages: an attachment receptor and an uncoating receptor (9). In this study, CVB3Q could utilize the dual-receptor system (CD55 as the attachment receptor and CAR as the uncoating receptor) to accomplish viral entry. For CVB3E, CAR was a bifunctional receptor that fulfilled both steps. Each CD55 molecule bridged two adjacent protomers of the CVB3 viral capsid, allowing the canyon to overlap CD55 and CAR (*SI Appendix*, Fig. S5*D*). Coyne and Bergelson reported that the CVB3 attachment to CD55 on the apical cell surface activates specific signal transduction and permits virus movement to the tight junction (23). Within the junction, the virus interacts with CAR and promotes the uncoating process (23). In this way, CVB3Q/N/V isolates that can interact with CD55 may have priority in apical cell infection.

We observed that neutral pH could induce pocket factor release of CVB3 virions after binding to CAR, which is consistent with data from Xu et al. showing that CAR binding to the CVB1 virion canyon leads to viral uncoating under neutral pH (26). Hence, it is reasonable to suggest that the mature virus particles may transform into A particles on the cell membrane and provide an alternative pathway to entry into cells. Receptor-decorated liposome experiments showed that the uncoating and genome release efficiencies of CVB3Q were higher than those of CVB3E (*SI Appendix*, Fig. S9). CVB3Q uncoating operated in a pH-independent manner, whereas a low pH could favor CVB3E full-particle transmission to empty particles. These findings indicated that the release of the pocket factor and subsequent viral uncoating and genome release occurred under strain-dependent pH preferences, implying that the entry and infection of different enterovirus strains varied according to the extent of pH dependence. Interestingly, the same serotype CVB3 viruses that could use the same uncoating receptor and possessed highly conserved receptor binding sites still showed significant differences in pH preferences for viral uncoating. Although the underlying mechanism of action is not well-understood, these findings help explain the different phenomena detected in previous studies in which endosomal acidification conditions could affect several CVB3 infections but not all CVB3 isolates (36, 37). An acidic environment could trigger more significant conformational changes in the VP1 GH loop of some enterovirus virions (11, 12). This has been proposed as a sensor loop that can initiate a cascade of events, including the release of the pocket factor and the formation of A particles and empty particles (26). Additionally, temperature can affect the uncoating efficiency observed in some enteroviruses (13), indicating that the trigger mechanism for virus uncoating may be diverse.

In conclusion, we defined VP3-234 sites as a vital molecular switch controlling CD55 binding to CVB3 virions during viral adaptive evolution. The findings provide a critical criterion to assess whether a newly isolated clinical CVB3 virus can utilize a dual receptor or single bifunctional receptor to enter and infect cells. Moreover, a series of molecular events at different stages of viral infection demonstrated the dynamic cell-entry mechanism of CVB3 and the function of the uncoating receptor CAR with strain-dependent pH preferences. Taken together, these findings expand the understanding of the mechanism underlying nonenveloped virus infection and provide clues for developing antiviral therapeutics.

Materials and Methods

Cells and Viruses. Human rhabdomyosarcoma, HEp-2, and HEK293T cells were maintained at 37 °C in an atmosphere of 5% CO_2 in minimal essential medium (Gibco) supplemented with 10% fetal bovine serum (Invitrogen) and penicillin-streptomycin. CVB3Q (VP3-234Q, MKP, which can induce mouse myocarditis) was obtained from Jilin University. CVB3N (VP3-234N, XJ12-36/XJ/CHN/2012, mild case of HFMD), CVB3E (VP3-234E XZ17-10/XZ/CHN/2017, healthy children), CVB3V (VP3-234V, GS12-55/GS/CHN/2012, severe cases of HFMD), and CVB3D (VP3-234D, HuN16-54/HuN/CHN/2016, fatal case of HFMD) strains were provided by the National Institute for Viral Disease Control and Prevention, Chinese Center for Disease Control and Prevention. CVB3Q, CVB3N, and CVB3V strains were propagated in rhabdomyosarcoma cells. CVB3D and CVB3E were propagated in HEp-2 cells.

Virus Production and Purification. CVB3Q, CVB3V, and CVB3N strains were propagated in rhabdomyosarcoma cells at a multiplicity of infection (MOI) of 0.5 at 37 °C. CVB3Q virus was collected 36 h after infection. CVB3N and CVB3V strains were collected 48 h after infection. CVB3D and CVB3E isolates were propagated in HEp-2 cells for 48 h at 37 °C after inoculation with an MOI of 0.5. CVB3Q, CVB3N, CVB3V, CVB3D, and CVB3E culture supernatants were centrifuged at 8,500 × *g* for 70 min to remove cell debris and concentrated using a hollow fiber ultrafiltration membrane (300 kDa). Initial purification was performed by ultracentrifugation at 120,000 × *g* for 2.5 h. The virus was resuspended in phosphate-buffered saline (PBS, pH 7.4) and then sedimented through a linear 20 to 45% (weight/volume; wt/vol) sucrose gradient at 140,000 × *g* for 4 h at 4 °C. Fractions containing viral particles were pooled, buffer-exchanged to PBS, and concentrated using an Amicon Ultra-6 100-kDa cutoff centrifugal concentrator (Millipore). CVB3Q, CVB3N, CVB3V, CVB3D, and CVB3E virion quantity and quality were examined by negative-staining EM with an FEI Tecnai G20 transmission electron microscope operating at 120 kV.

Protein Expression and Purification. CAR (residues 20 to 236) coding sequences were cloned into the pET21a vector (Invitrogen) and six histidine residues at the C terminus into *Nde*I and *Xho*I restriction sites. Recombinant proteins were expressed in *Escherichia coli* strain BL21 (DE3) as inclusion bodies and refolded as previously described (14). The proteins were subsequently purified by gel filtration using a Superdex 200 100/300 GL column (GE Healthcare) with a buffer containing 20 mM Tris·HCl and 150 mM NaCl (pH 8.0). The soluble CD55 extracellular domain was prepared as previously described (11). The complementary DNA sequence encoding the CD55 extracellular domain (residues D35 to G285) was cloned into the pCMV3 vector with a human interleukin-2 signal sequence at the N terminus and six histidine residues at the C terminus. Proteins were purified by nickel affinity chromatography and gel filtration using a HiLoad 100/300 Superdex 200 GL column (GE Healthcare) with a buffer containing 20 mM Tris·HCl and 150 mM NaCl (pH 8.0).

SPR. SPR analysis was performed using a BIAcore 3000 device (GE Healthcare) with an SA sensor chip (GE Healthcare) at room temperature. All viruses used were first biotinylated with NHS-biotin reagent with a molar ratio of ~3:1 and then exchanged into PBS buffer with a 100-kDa centrifugal concentrator. Biotinylated viruses were individually immobilized on different channels of the SA chip to ~6,500 response units. CAR and CD55 receptor proteins were serially diluted in pH 7.4 buffer consisting of PBS and 0.005% (vol/vol) Tween-20 (PBST) and 2-(*N*-morpholino)ethanesulfonic acid (MES) at pH 5.5 (20 mM MES, 150 mM NaCl) and 0.005% (vol/vol) Tween-20 (MEST), respectively. Serially diluted analytes flowed through the chip at a rate of 30 μL/min. After a single cycle, a short injection of 2 M $MgCl_2$ was used to regenerate the sensor surface. Binding kinetics were analyzed using BIA evaluation software, version 4.1.

Sample Preparation and Cryo-EM Data Collection. Purified virus particles were incubated with excess CD55 protein for 20 min and with CAR for 10 min on ice. A 3-μL aliquot of free CVB3 virus or CVB3–CD55 or CVB3–CAR complex at pH 7.4 was applied to a glow-discharged ultrathin carbon-coated copper grid. The grid was blotted for 2.5 s in 100% relative humidity and plunge-frozen in liquid ethane using a Vitrobot Mark IV. Low-pH samples were handled by adding 3 μL acid buffer (20 mM MES and 150 mM NaCl, pH 5.5) to the grid after the first blotting. Samples were incubated for an additional 10 min at 4 °C before blotting and plunge freezing. Cryo-EM data were collected at 300 kV with an FEI Titan Krios equipped with a Falcon 3 camera. Each movie of 32 frames was exposed for 1 s, with an exposure time of ~0.031 s per frame. The total dose was ~40 $e^-/Å^2$. The defocus value was set from −2.5 to −1.0 μm with a pixel size of 1.08 Å.

Image Processing, Model Building, and Refinement. Image stacks were corrected for beam-induced motion using MotionCor2 (38). Contrast transfer function parameters were estimated using CTFFIND4 (39). Good micrographs were selected based on Thon rings. Particles were automatically boxed using the ethan.py tool in the EMAN program package (40). After that, the 4× binned particle images were extracted and subjected to reference-free two-dimensional (2D) classification with RELION-3.0.8. After several rounds of 2D classification, bad particles were eliminated. The coordinates for good particles were used to extract the 2× binned particles for three-dimensional (3D) classification with I3 symmetry. The target classes with ideal resolution and particle numbers were selected to extract full-size particles for Refine3D, using the corresponding resultant maps from Class3D as the reference. After RELION postprocessing, resolution values were estimated by the gold-standard Fourier shell correlation cutoff value of 0.143. For the CVB3Q_Full_pH7.4 dataset, the CVB3Q_Full density map was obtained at the resolution of 2.95 Å. In addition, A particles and empty particles were acquired with 3.3- and 3.53-Å resolution, respectively. The relevant A particle density maps were also acquired with the CVB3N_CD55_pH7.4, CVB3Q_CAR_10min_pH7.4, and CVB3Q_CAR_20-min_pH5.5 datasets. For the CVB3N_Full_pH7.4 and CVB3E_CAR_10min_pH7.4 datasets, CtfRefine was executed to improve the quality of the final maps (*SI Appendix*, Figs. S2 and S6). The crystal structure of the CVB3 coat protein (Protein Data Bank ID code 1COV) was used as the initial model to fit into the CVB3Q_Full (pH 7.4) density map using the Chimera program (41). Model accuracy was manually adjusted in Coot (42) for improvement. An asymmetric unit density map was segmented using Chimera (41). The models were further improved by real space refinement using Phenix (43). Other models were built based on the model of CVB3Q_Full, following a similar procedure as described above. Chimera was used to visualize the cryo-EM maps and render EM density figures (41). Graphical representations of atomic models were generated using PyMOL or the Chimera program package.

Preparation of Receptor-Decorated Liposomes. Liposomes consisting of phosphatidylethanolamine, phosphatidylcholine, sphingomyelin, cholesterol, and phosphatidic acid were dissolved in chloroform and mixed in molar ratios of 1:1:1:1.5:0.3, respectively. The detailed procedure has been previously described (11). Nickel-chelating liposomes were prepared by extruding lipids through a membrane filter with 0.4-mm-diameter pores and then incubating with His-tagged CD55 or CAR at a final concentration of 50 mg/mL at room temperature for 30 min.

Incubation Assay of Receptor-Decorated Liposomes with CVB3 Particles. High-purity CVB3Q and CVB3E full particles were obtained by 20 to 45% (wt/vol) sucrose density gradient centrifugation. Next, 20 μL of receptor-decorated liposomes and CVB3 full particles was incubated at pH 7.4 for 10 min on ice. The virus/receptor mixtures were divided into two equal parts. Ten microliters of neutral buffer (pH 7.4, PBS buffer) and 10 μL of acidic buffer (20 mM MES and 150 mM NaCl, pH 3.8) were added separately to these two samples to ensure that the pH of the two equal buffers was maintained at 7.4 (neutral condition) and 5.5 (acidic condition). After incubation for 10, 30, and 60 min, the mixed samples were used for negative staining. The specimens were loaded onto the FEI Tecnai G20 transmission electron microscope operating at 120 kV for imaging. The statistics of each sample were calculated using Prism with ~500 total particles from randomly selected images. The significance of differences was tested using Tukey's multiple-comparison test implemented in GraphPad Prism software.

Data Availability. The density maps for this article have been deposited in the Electron Microscopy Data Bank with accession nos. EMD-32179 (full CVB3Q, pH 7.4), EMD-32190 (full CVB3N, pH 7.4), EMD-32251 (full CVB3E, pH 7.4), EMD-32194 (CVB3Q_CD55, pH 7.4), EMD-32195 (CVB3N_CD55, pH 7.4), EMD-32207 (CVB3Q_CAR, 10 min, pH 7.4), EMD-32189 (CVB3Q_CAR, 20 min, pH 7.4), EMD-32208 (CVB3Q_CAR, 20 min, pH 5.5), EMD-32209 (CVB3E_CAR, 10 min, pH 7.4), and EMD-32250 (CVB3E_CAR, 20 min, pH 7.4). The coordinates of the corresponding atomic models have been deposited in the Protein Data Bank with ID codes 7VXH (full CVB3Q, pH 7.4), 7VY0 (full CVB3N, pH 7.4), 7W17 (full CVB3E, pH 7.4), 7VY5 (CVB3Q_CD55, pH 7.4), 7VY6 (CVB3N_CD55, pH 7.4), 7VYK (CVB3Q_CAR, 10 min, pH 7.4), 7VXZ (CVB3Q_CAR, 20 min, pH 7.4), 7VYL (CVB3Q_CAR, 20 min, pH 5.5), 7VYM (CVB3E_CAR, 10 min, pH 7.4), and 7W14 (CVB3E_CAR, 20 min, pH 7.4).

All study data are included in the article and/or *SI Appendix*.

ACKNOWLEDGMENTS. We acknowledge the support of the Hong Kong Institute for Advanced Studies. We thank all staff members at the Cryo-EM Centre of the Southern University of Science and Technology for their assistance with cryo-EM data collection. We express special thanks to Dr. Zheng Fan and Dr. Wei Zhang of the Institute of Microbiology, CAS, for their assistance with the SPR experiments. We are grateful to Kaiming Zhang of the Department of Bioengineering, Stanford University, for image processing and reconstruction. This work was supported by the Strategic Priority Research Program of the CAS (XDB29010202), National Science Foundation of China (82072289), National Key R&D Program of China (2020YFA0509202), and Shaanxi Provincial Education Department (203012100077).

1. D. Lugo, P. Krogstad, Enteroviruses in the early 21st century: New manifestations and challenges. *Curr. Opin. Pediatr.* **28**, 107–113 (2016).
2. I. Gaaloul *et al.*, Coxsackievirus B detection in cases of myocarditis, myopericarditis, pericarditis and dilated cardiomyopathy in hospitalized patients. *Mol. Med. Rep.* **10**, 2811–2818 (2014).
3. K. Vehik *et al.*, TEDDY Study Group, Prospective virome analyses in young children at increased genetic risk for type 1 diabetes. *Nat. Med.* **25**, 1865–1872 (2019).
4. H. Hyöty, F. Leon, M. Knip, Developing a vaccine for type 1 diabetes by targeting coxsackievirus B. *Expert Rev. Vaccines* **17**, 1071–1083 (2018).
5. A. H. Wong, C. S. Lau, P. K. Cheng, A. Y. Ng, W. W. Lim, Coxsackievirus B3-associated aseptic meningitis: An emerging infection in Hong Kong. *J. Med. Virol.* **83**, 483–489 (2011).
6. Z. Han *et al.*, Two coxsackievirus B3 outbreaks associated with hand, foot, and mouth disease in China and the evolutionary history worldwide. *BMC Infect. Dis.* **19**, 466 (2019).
7. G. R. Abedi, J. T. Watson, W. A. Nix, M. S. Oberste, S. I. Gerber, Enterovirus and parechovirus surveillance—United States, 2014–2016. *MMWR Morb. Mortal. Wkly. Rep.* **67**, 515–518 (2018).
8. K. I. Calderón *et al.*, Molecular epidemiology of coxsackievirus B3 infection in Spain, 2004–2014. *Arch. Virol.* **161**, 1365–1370 (2016).
9. M. G. Rossmann, Y. He, R. J. Kuhn, Picornavirus-receptor interactions. *Trends Microbiol.* **10**, 324–331 (2002).
10. J. M. Bergelson, C. B. Coyne, Picornavirus entry. *Adv. Exp. Med. Biol.* **790**, 24–41 (2013).
11. X. Zhao *et al.*, Human neonatal Fc receptor is the cellular uncoating receptor for enterovirus B. *Cell* **177**, 1553–1565.e16 (2019).
12. Y. Cui *et al.*, Molecular basis of coxsackievirus A10 entry using the two-in-one attachment and uncoating receptor KRM1. *Proc. Natl. Acad. Sci. U.S.A.* **117**, 18711–18718 (2020).
13. M. Strauss *et al.*, Nectin-like interactions between poliovirus and its receptor trigger conformational changes associated with cell entry. *J. Virol.* **89**, 4143–4157 (2015).
14. A. M. Milstone *et al.*, Interaction with coxsackievirus and adenovirus receptor, but not with decay-accelerating factor (DAF), induces A-particle formation in a DAF-binding coxsackievirus B3 isolate. *J. Virol.* **79**, 655–660 (2005).
15. S. D. Carson, Kinetic models for receptor-catalyzed conversion of coxsackievirus B3 to A-particles. *J. Virol.* **88**, 11568–11575 (2014).
16. K. Wang *et al.*, Structures of echovirus 30 in complex with its receptors inform a rational prediction for enterovirus receptor usage. *Nat. Commun.* **11**, 4421 (2020).
17. J. Baggen, H. J. Thibaut, J. R. P. M. Strating, F. J. M. van Kuppeveld, The life cycle of non-polio enteroviruses and how to target it. *Nat. Rev. Microbiol.* **16**, 368–381 (2018).
18. J. K. Pfeiffer, K. Kirkegaard, Increased fidelity reduces poliovirus fitness and virulence under selective pressure in mice. *PLoS Pathog.* **1**, e11 (2005).

19. Y. Wang, J. K. Pfeiffer, Emergence of a large-plaque variant in mice infected with coxsackievirus B3. *mBio* **7**, e00119 (2016).
20. M. Vignuzzi, J. K. Stone, J. J. Arnold, C. E. Cameron, R. Andino, Quasispecies diversity determines pathogenesis through cooperative interactions in a viral population. *Nature* **439**, 344–348 (2006).
21. J. Pan *et al.*, Single amino acid changes in the virus capsid permit coxsackievirus B3 to bind decay-accelerating factor. *J. Virol.* **85**, 7436–7443 (2011).
22. A. V. Novoselov *et al.*, A single amino acid substitution controls DAF-dependent phenotype of echovirus 11 in rhabdomyosarcoma cells. *Virus Res.* **166**, 87–96 (2012).
23. C. B. Coyne, J. M. Bergelson, Virus-induced Abl and Fyn kinase signals permit coxsackievirus entry through epithelial tight junctions. *Cell* **124**, 119–131 (2006).
24. D. Zhou *et al.*, Unexpected mode of engagement between enterovirus 71 and its receptor SCARB2. *Nat. Microbiol.* **4**, 414–419 (2019).
25. S. Niu *et al.*, Molecular and structural basis of echovirus 11 infection by using the dual-receptor system of CD55 and FcRn [in Chinese]. *Chin. Sci. Bull.* **65**, 67–79 (2020).
26. L. Xu *et al.*, Cryo-EM structures reveal the molecular basis of receptor-initiated coxsackievirus uncoating. *Cell Host Microbe* **29**, 448–462.e5 (2021).
27. N. L. Kallewaard *et al.*, Tissue-specific deletion of the coxsackievirus and adenovirus receptor protects mice from virus-induced pancreatitis and myocarditis. *Cell Host Microbe* **6**, 91–98 (2009).
28. J. Pan, L. Zhang, L. J. Organtini, S. Hafenstein, J. M. Bergelson, Specificity of coxsackievirus B3 interaction with human, but not murine, decay-accelerating factor: Replacement of a single residue within short consensus repeat 2 prevents virus attachment. *J. Virol.* **89**, 1324–1328 (2015).
29. S. H. Dho, J. C. Lim, L. K. Kim, Beyond the role of CD55 as a complement component. *Immune Netw.* **18**, e11 (2018).
30. S. H. Dho *et al.*, A novel therapeutic anti-CD55 monoclonal antibody inhibits the proliferation and metastasis of colorectal cancer cells. *Oncol. Rep.* **42**, 2686–2693 (2019).
31. H. Zhou, H. Hara, D. K. C. Cooper, The complex functioning of the complement system in xenotransplantation. *Xenotransplantation* **26**, e12517 (2019).
32. M. G. Detsika *et al.*, Induction of decay accelerating factor and membrane cofactor protein by resveratrol attenuates complement deposition in human coronary artery endothelial cells. *Biochem. Biophys. Rep.* **19**, 100652 (2019).
33. K. Fujii *et al.*, VP1 amino acid residue 145 of enterovirus 71 is a key residue for its receptor attachment and resistance to neutralizing antibody during cynomolgus monkey infection. *J. Virol.* **92**, e00682-18 (2018).
34. K. Kobayashi *et al.*, Amino acid variation at VP1-145 of enterovirus 71 determines attachment receptor usage and neurovirulence in human scavenger receptor B2 transgenic mice. *J. Virol.* **92**, e00681-18 (2018).
35. Y. Nishimura *et al.*, Enterovirus 71 binding to PSGL-1 on leukocytes: VP1-145 acts as a molecular switch to control receptor interaction. *PLoS Pathog.* **9**, e1003511 (2013).
36. K. P. Patel, C. B. Coyne, J. M. Bergelson, Dynamin- and lipid raft-dependent entry of decay-accelerating factor (DAF)-binding and non-DAF-binding coxsackieviruses into nonpolarized cells. *J. Virol.* **83**, 11064–11077 (2009).
37. S. K. Chung *et al.*, Internalization and trafficking mechanisms of coxsackievirus B3 in HeLa cells. *Virology* **333**, 31–40 (2005).
38. S. Q. Zheng *et al.*, MotionCor2: Anisotropic correction of beam-induced motion for improved cryo-electron microscopy. *Nat. Methods* **14**, 331–332 (2017).
39. A. Rohou, N. Grigorieff, CTFFIND4: Fast and accurate defocus estimation from electron micrographs. *J. Struct. Biol.* **192**, 216–221 (2015).
40. S. J. Ludtke, P. R. Baldwin, W. Chiu, EMAN: Semiautomated software for high-resolution single-particle reconstructions. *J. Struct. Biol.* **128**, 82–97 (1999).
41. E. F. Pettersen *et al.*, UCSF Chimera—A visualization system for exploratory research and analysis. *J. Comput. Chem.* **25**, 1605–1612 (2004).
42. P. Emsley, K. Cowtan, Coot: Model-building tools for molecular graphics. *Acta Crystallogr. D Biol. Crystallogr.* **60**, 2126–2132 (2004).
43. P. D. Adams *et al.*, PHENIX: A comprehensive Python-based system for macromolecular structure solution. *Acta Crystallogr. D Biol. Crystallogr.* **66**, 213–221 (2010).